

# Assessing Artificial Groundwater Recharge on Irrigated Land Using the MODFLOW Model

## *A Case Study from Karatal Agricultural Area, Kazakhstan*

Vladimir Mirlas<sup>1</sup>, Valery Antonenko<sup>2</sup>, Vitaly Kulagin<sup>3</sup> & Elmira Kuldeeva<sup>2</sup>

<sup>1</sup> Agro-Ecology Research & Development LTD, Rubicon Business Group, Israel

<sup>2</sup> Department of Hydrogeology, Kazakhstan National Technical University in the name of K.I. Satpayev, Kazakhstan

<sup>3</sup> Zonal Hydrogeological Reclamation Center of Kazakhstan, Kazakhstan

Correspondence: Vladimir Mirlas, Agro-Ecology Research & Development LTD, Rubicon Business Group, 98 Yigal Allon St., Tel-Aviv 6789141, Israel. Tel: 972-524-831-024. E-mail: vladimirmster@gmail.com

Received: December 17, 2014 Accepted: March 4, 2015 Online Published: March 20, 2015

doi: 10.5539/esr.v4n2p16 URL: <http://dx.doi.org/10.5539/esr.v4n2p16>

*The research is financed by the Ministry of Education and Science of the Kazakhstan Republic under research grant #38.61.05.*

### Abstract

Water-resource deficits have led to the need for artificial groundwater-recharge techniques to provide drinking water for rural communities in southeastern Kazakhstan, especially those with a small number of inhabitants. The Kishi-Tobe settlement located in the Karatal agricultural area on the right bank of the Karatal River in southeastern Kazakhstan has severe water-supply shortages. In this study, the groundwater-flow model MODFLOW was used to simulate complex hydrogeological and irrigation conditions for a quantitative assessment of artificial groundwater recharge from infiltration pools. The aim of these pools was to solve the water shortage in the Kishi-Tobe settlement. New findings showed that the maximum rate of artificial groundwater recharge from the infiltration pool can reach  $1000 \text{ m}^3 \text{ day}^{-1}$ , corresponding to an infiltration rate of  $0.2 \text{ m day}^{-1}$ , which creates a groundwater mound with a radius of around 500 m from the center of the pool. The groundwater mound also serves as a hydrodynamic barrier, preventing inflow of contaminated groundwater from irrigated fields and rice checks to the pumping wells. The potential rate of groundwater pumping from two water-supply wells can reach up to  $7350 \text{ m}^3 \text{ day}^{-1}$  over 10 years, providing a maximum drawdown in the wells of about 24 m. The water required by the Kishi-Tobe settlement can be supplied at a rate of  $864 \text{ m}^3 \text{ day}^{-1}$ , achieving both available drawdowns by the end of the forecast period and balanced provision of the groundwater resource.

**Keywords:** artificial recharge, irrigation, numerical model, water supply

### 1. Introduction

The water-resource deficit in southeastern Kazakhstan, compounded by the large distances to natural water sources of good quality, requires the combined use of reservoirs and groundwater from local aquifers to supply the local population with good-quality drinking water. Under these conditions, application of artificial groundwater-recharge techniques can be an efficient way to provide the rural communities with drinking water, especially those with a small number of inhabitants. The groundwater resources can be significantly increased and the salinity of the water may be decreased, thus enhancing both quantity and quality of the drinking water.

Artificial recharge methods have been proven efficient at maintaining and replenishing aquifers (Fred, 2006). The existing methods of artificially recharging aquifers, such as infiltration basins and canals, water traps, surface-runoff drainage wells, and diversion of excess flow from irrigation canals, among others, have been reviewed by Kavuri, Boddu, and Annamdas (2011).

Al-Turbak (1991) found that during surface reservoir recharging to an underlying unconfined aquifer located in central Saudi Arabia, 82% to 94.5% of the stored water was taken into the soil. Bloyd (1971) showed that it is

technically feasible to store imported water without causing water logging in the storage area and without losing any significant quantity of the stored water. Koch (1984) showed total water recharge into the aquifer of Big Sioux River over 120 days amounting to 150.3 million gallons, with 36% of this discharged from the aquifer to the river.

Common approaches to research and design systems for the artificial recharge of groundwater have been described by Bouwer (2002). That author noted that artificial recharge, resulting in the conjunctive use of surface water, is preferred whenever possible. Furthermore, artificial recharge plays an important role in water reuse, because it provides quality benefits (e.g. soil aquifer treatment) and storage opportunities that can absorb the seasonal differences between water supply and demand. The design and management of artificial recharge systems involves geological, geochemical, hydrological, biological, and engineering aspects. In the initial stages of designing large artificial recharge systems, it is advisable to conduct research on pilot and small-scale systems until the complete system can be designed and constructed.

In evaluating the recharge efficiency of a surface reservoir, it is important to know at the outset how much of the stored water infiltrates from the bottom of the reservoir. One way to quantify this is to apply a water-budget approach (Evans, Young, & Onyskow, 1983; Khan & Mawdsley, 1984). Another way is to apply computer modeling. Various computer models are now widely used to provide solutions for the assessment of artificial groundwater recharge. The common approach of numerical groundwater modeling to estimate regional recharge rates has been described by Sanford (2002).

Predictive modeling of groundwater abstraction and artificial recharge of cooling water was performed using the reactive transport model SHEMAT (Simulator for HEat and MAass Transport) (Gandy, Clarke, & Banks, 2010). A series of simulations were undertaken to determine the optimum configuration of the abstraction and recharge boreholes, so as to minimize the effects on the aquifer. Gropius (2010) noted that computer models of groundwater flow and heat transport are essential to predicting the hydraulic and thermal impacts of the proposed open-loop ground source heating systems on ground- and surface-water ecosystems. In that paper, conceptual models and numerical heat-transport modeling strategies to predict the performance of sustainable long-term ground-source heat schemes, and assess their impact on other groundwater users in the London Chalk aquifer, were discussed. Water-balance calculations and groundwater modeling were utilized to study an improved water-harvesting technique termed floodwater spreading system in arid Iran (Hashemi, Berndtsson, & Persson, 2014). That research showed that the floodwater-spreading system can efficiently increase groundwater resources in arid and semi-arid areas.

Salinization of irrigated lands is a common phenomenon wherever irrigation is practiced under arid or semi-arid climatic conditions. Different drainage systems constitute the widely used solutions for these phenomena. A comparison between horizontal and vertical drainage systems, including pipe drainage, open-ditch drainage, and pumped wells in anisotropic soils was studied by Valipour (2012a, 2013). Knowledge of the effects of changes in drainage parameters on drain discharge is essential in subsurface drainage systems (Valipour, 2012b). The essential problems related to drainage engineering, covering both urban and agricultural drainage systems, are described in the Handbook of Drainage Engineering Problems (Valipour, 2014).

The groundwater-flow model MODFLOW has been used to solve complex drainage problems in irrigated fields in Israel (Mirlas, 2009, 2012, 2013). This model of the spatial distribution of groundwater flow has provided additional information for the planning of effective subsurface drainage systems under complex hydrogeological and intensive farming conditions in irrigated fields. The model has improved researchers' knowledge of spatial recharge of the groundwater through percolation of rainfall and irrigation water.

The objective of this study was the quantitative assessment of artificial groundwater recharge from infiltration pools under irrigation conditions to solve the water-supply problems of the local rural communities in the Karatal agricultural area in Kazakhstan. MODFLOW was used as a tool for numerical simulations. The hydrogeochemical aspects of artificial groundwater recharge from the infiltration basins will be the subject of future research.

## **2. Materials and Methods**

### *2.1 Geographical and Hydrological Conditions at the Research Site*

The Karatal agricultural area is located on the right bank of the Karatal River in southeastern Kazakhstan, about 5 km north of the town of Ushtobe, and covers nearly 250 km<sup>2</sup> (Figure 1). In geomorphological terms, it is a flat alluvial plain, extending between the Karatal and Aksu rivers in the Lake Balkhash basin. Surface elevations of the Karatal agricultural area range from 427 m (above mean sea level) in the southern part of the area to 417 m

in its northern part and near the bank of the Karatal River.

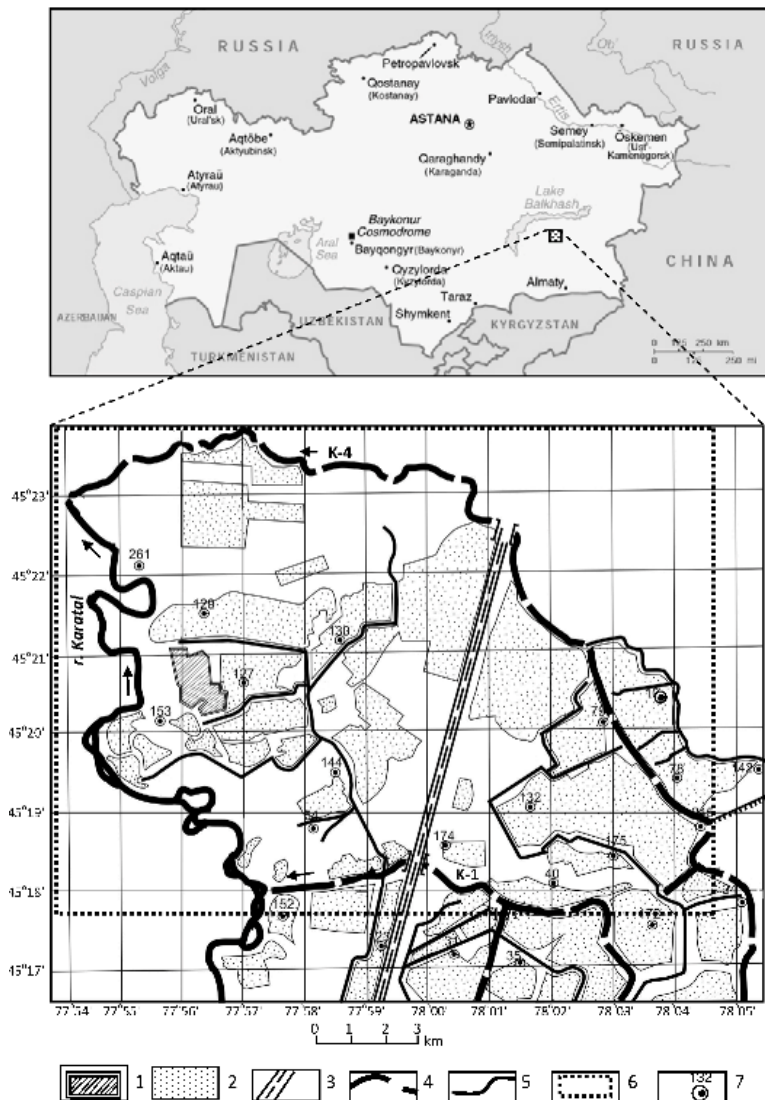


Figure 1. Location of Karatal irrigated fields. Numbers in legend indicate the following locations on the map: 1 = Kishi-Tobe settlement; 2 = irrigated fields; 3 = road; 4 = main drainage canals; 5 = irrigation canals; 6 = model domain; 7 = observation wells. Regional map of Kazakhstan was taken from open internet site <http://www.ed-u.com/kz.html>

The Karatal agricultural area is classified as a zone of sharply continental climate, characterized by harsh winters, hot summers, short spring and autumn, low air humidity, and a relatively small amount of precipitation. Absolute minimum and maximum temperatures are recorded in January ( $-17.7\text{ }^{\circ}\text{C}$ ) and in July ( $+24.3\text{ }^{\circ}\text{C}$ ), respectively. Annual precipitation is around 250 mm, 40% of it falling during the spring–summer period (April–July).

The Karatal River originates from the northwestern slopes of the Zhongar Alatau mountains. It is 327 km long and its catchment basin covers  $14\,200\text{ km}^2$ . Average annual water discharge in the Karatal River, measured near Ushtobe, is  $68.4\text{ m}^3\text{ s}^{-1}$ , with maximum and minimum values of  $120\text{ m}^3\text{ s}^{-1}$  and  $32.4\text{ m}^3\text{ s}^{-1}$ , respectively. River flooding occurs in May and June. Total water salinity of the Karatal River ranges between 199 and  $237\text{ mg l}^{-1}$ . The water type is calcium bicarbonate.

Water from the Karatal River is used for irrigation. The water is supplied by Ushtobe's main irrigation canal and by secondary irrigation canals serving the irrigated fields. A system of drainage canals is used to drain excess irrigation and drainage water from the irrigated fields. Through the main drainage canals K-1 and K-4, the drained water flows back into the Karatal River. In 2012, the total water supply for irrigation was  $35.9 \times 10^6\text{ m}^3$

and the total volume of drained water was  $13.2 \times 10^6 \text{ m}^3$ . The main agricultural crop in the area is rice. The rice checks (paddy fields) cover about 370 ha, each rice check averaging 2.1 ha. The height of the wall bulk rice check is 0.7 m and the thickness at the bottom is 0.8 m. The height of the water layer in the rice checks after seeding (30 Apr–31 May) is 10 cm, during tillering (05 Jun–15 Jul) it is 15 cm, and during the milky wax ripeness stage (20 Aug–05 Sep) it is 12 cm. Rice ripening usually takes 135 days, and harvesting begins in mid-September. Associated crops are wheat, alfalfa and vegetables.

The Kishi-Tobe settlement located in the Karatal agricultural area has about 500 inhabitants; according to regional plans, the population is expected to grow. Currently, water is supplied to local residents from the Karatal River, with no preliminary treatment.

The Quaternary alluvial deposits within the Karatal agricultural area, with an average thickness of 55 m, are mostly composed of sand with lenses and layers of clay and loam. They include two hydrodynamically interconnected aquifers planned for use as a water supply for the Kishi-Tobe settlement.

The upper unconfined aquifer of the undifferentiated contemporary and middle Quaternary alluvial deposits is comprised of silty loam, fine sands and clayey silts. The average thickness of the aquifer ranges from 5 to 12 m. Hydraulic conductivity values vary from 1 to  $3.4 \text{ m day}^{-1}$ . The depth of the groundwater level approximately mirrors the landforms and decreases from 5 m to 2 m in the northwest direction (Shakibaev, Kulagin, & Zaharova, 2013). The aquifer groundwater is mainly fresh, characterized by salinity up to  $0.5 \text{ g l}^{-1}$ .

The underlying semi-confined aquifer of the undifferentiated middle and lower Quaternary alluvial and lacustrine-alluvial deposits is widespread in the Karatal agricultural area and considered to be the most relevant water-supply source. The aquifer is comprised of fine- and medium-grained sand with gravel and with frequent lenses of medium-dense clay. Lenses and layers of clay and loam create conditions for local groundwater pressure head. The aquifer thickness varies from 15 to 60 m, increasing in a northwesterly direction. Groundwater levels are located at depths ranging from 3 to 12 m from the soil surface. Hydraulic conductivity values of the aquifer vary from 4 to  $10 \text{ m day}^{-1}$ . Groundwater of the aquifer is mainly fresh with salinity up to  $1.0 \text{ g l}^{-1}$ . The main direction of groundwater flow is northwest toward the Karatal River. The hydraulic gradient varies from 0.0002 to 0.001, increasing near the Karatal River. Intensive irrigation significantly affects groundwater-flow patterns during the summer. A groundwater mound forms under and near the flooded rice fields. The hydraulic gradient near the rice checks increases and the groundwater also flows toward the main drainage canals.

## 2.2 Methods

### 2.2.1 Hydrogeological Survey

A survey of the hydrogeological conditions to assess groundwater resources, dynamics, and parameters required for modeling was carried out by the Zonal Hydrogeological Reclamation Center of the Kazakhstan Republic (Shakibaev et al., 2013). The hydrogeological survey included:

- 1) drilling and installation of twelve 6- to 12-m deep observation wells (Figure 1): each 3-inch diameter observation well was equipped with a 1-m long slotted screen installed in the lower part of the well;
- 2) pumping tests (Kruseman & De Ridder, 1976) to estimate the hydraulic conductivity values of the aquifer: double-ring infiltrometer tests were carried out in four 1.0-m deep boreholes to estimate the saturated hydraulic conductivity of the upper unsaturated zone of the aquifer;
- 3) groundwater level and salinity monitoring during 2011–2012: water-table depths were measured once a month; water sampling from each observation well was carried out twice a year, in the spring and autumn; water chemical analyses were performed for pH, TDS (total dissolved solids), and Ca, Mg, Na + K, Cl,  $\text{SO}_4$ , and  $\text{HCO}_3$  concentrations; the sodium adsorption ratio (SAR) was calculated based on laboratory analysis;
- 4) recording of precipitation, irrigation rates, drainage-water discharge, potential evaporation, and crop rotation in the fields; water and salt balances for 2011–2012 were calculated for three different irrigation systems of the Karatal irrigated area;
- 5) measurement of the Karatal River discharge once a month using the gauging station located at the river outlet to the irrigated area; water sampling from the Karatal River was carried out in April and September 2011 and in April, June, August and September 2012 to identify chemical composition (pH, TDS, Ca, Mg, Na + K, Cl,  $\text{SO}_4$ , and  $\text{HCO}_3$ ) of the river water.

Based on the results of the hydrogeological survey, the following data were prepared for modeling the hydrogeological conditions of the irrigated Karatal fields:

- topographic map of the Karatal River, main surface drainage and irrigation canals, coordinates of the observation wells, and soil surface elevation;
- contour maps of the aquifer's lower boundaries;
- land-use maps showing irrigated fields, rice checks and types of crops;
- set of overlapping hydrogeological cross sections showing lithological structure of deposits comprising the aquifers, and the areal and vertical extent of the model boundaries;
- hydraulic head maps for each aquifer;
- map of water-table depth from the soil surface;
- hydraulic conductivity and storage property values obtained by pumping and infiltrometer tests;
- spatial and temporal data of groundwater levels and chemical composition of groundwater obtained during monitoring;
- hydrographs of the Karatal River and main drainage canals (K-1 and K-4);
- annual soil–water balance, irrigation regime of the crops and rice check data.

### 2.2.2 Methodology

The MODFLOW groundwater model was used to simulate temporal and spatial changes in groundwater under existing hydrogeological and irrigation conditions. The calibrated model was applied to assess the changes in hydrogeological conditions and natural groundwater resources when setting the infiltration pool at the specified location, size, and mode of infiltration for a 10-year forecast period. Pumping of groundwater was simulated to account for the water supply required by the Kishi-Tobe agricultural settlement.

### 2.2.3 Mathematical Model

A mathematical model for the groundwater flow was described by partial differential equation of the three-dimensional groundwater flow for both unconfined and semi-confined aquifers.

For the upper unconfined aquifer:

$$\frac{\partial}{\partial x}[K_x(H_x - \eta_x)(\frac{\partial H}{\partial x})] + \frac{\partial}{\partial y}[K_y(H_y - \eta_y)(\frac{\partial H}{\partial y})] \pm W = S_y(\frac{\partial H}{\partial t}) \quad (1)$$

For the underlying semi-confined aquifers:

$$\frac{\partial}{\partial x}(K_x(\frac{\partial H}{\partial x})) + \frac{\partial}{\partial y}(K_y(\frac{\partial H}{\partial y})) \pm q = S_s(\frac{\partial H}{\partial t}) \quad (2)$$

where  $K_x$  and  $K_y$  = hydraulic conductivity along the  $x$ - and  $y$ -coordinate axes, respectively, which are the principal permeability directions;  $H$  = potentiometric head;  $\eta_x$  and  $\eta_y$  = elevation of the bottom of the unconfined aquifer along the  $x$ - and  $y$ -coordinate axes, respectively;  $W$  = fluxes that represent recharge, evaporation, pumping well, and drains;  $q$  represents the sources and/or sinks of water (pumping well, drains, and exchange between layers);  $S_y$  = specific yield of the porous material;  $S_s$  = specific storage of the porous material, and  $t$  = time.

Equations (1) and (2), together with the prescribed initial head and boundary conditions, represent the mathematical groundwater-flow model for the study area. The boundary conditions of the model are described in sections 2.2.4 and 2.2.5, specifying head, flux, and their combination. The groundwater-flow model of the Karatal-irrigated fields was constructed using Visual MODFLOW software, which is an integrated computer program package for simulation of three-dimensional groundwater flow (WHI, 2005).

### 2.2.4 Numerical Model

The model domain area was 20 424 x 10 820 m. To implement the numerical model, the study area was overlain by a grid composed of rectangular cells. The minimal size of the grid cells was 64 x 54 m at the infiltration pool and increased to 250 x 215 m in the southeastern part of the model domain. The total number of grid cells in two layers was 24 552 (Figure 2).

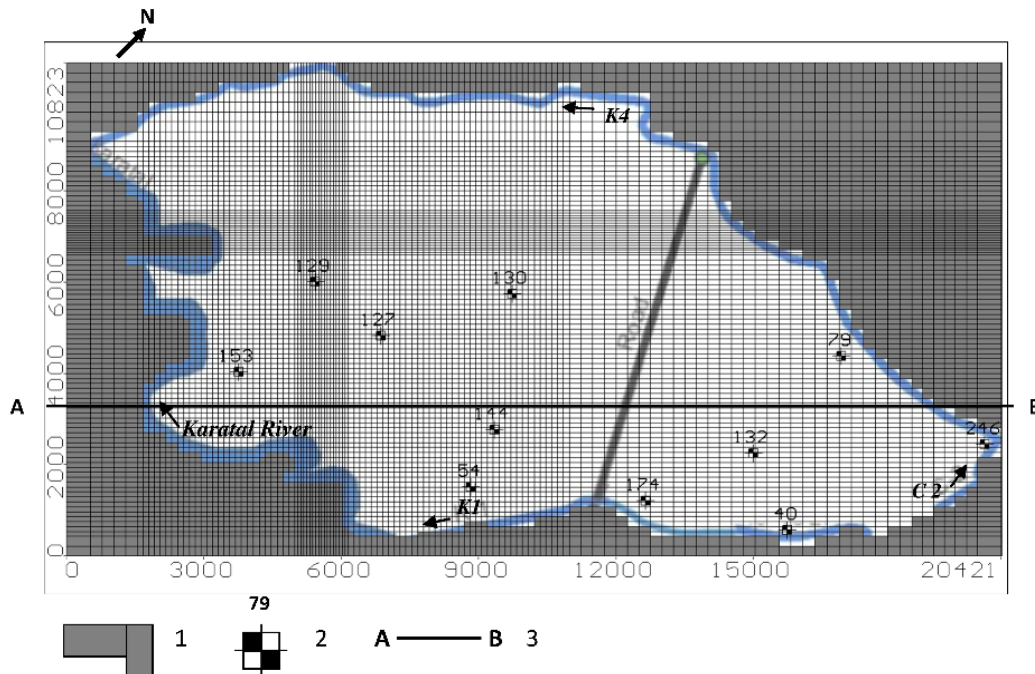


Figure 2. Finite difference grid of modeled Karatal area. Numbers in legend indicate the following locations on the map: 1 = inactive cells (no flow within model domain); 2 = observation well; 3 = cross-sectional line (for Figure 3)

The two-layered model represented the aquifer system as follows:

- Layer 1, upper unconfined aquifer comprised of the undifferentiated contemporary and middle Quaternary alluvial deposits (depth 3–8 m from soil surface), composed of silty loam, fine sands and clayey silts
- Layer 2, the underlying semi-confined aquifer of the undifferentiated middle and lower Quaternary alluvial and lacustrine-alluvial deposits, comprised of fine- and medium-grained sands with gravel and with frequent lenses of medium-dense clay.

Hydraulic conductivity values for Layer 1 were obtained from the pumping tests carried out in the shallow observation wells and the double-ring infiltrometer tests. They ranged from 0.5 to 1.2 m day<sup>-1</sup>, which is typical for the lithology of deposits in the study area. The thickness of Layer 2 was 30–55 m, based on information from the deep observation and geological survey wells. The hydraulic conductivity values of Layer 2 were obtained from the pumping tests performed in the deep observation wells. They varied from 3 to 11 m day<sup>-1</sup>, generally increasing to the north and toward the Karatal River.

The model boundaries were prescribed as follows: the western boundary was assigned along the Karatal River (from the main drainage canal K1 to the main northern drainage canal K4); the southern border followed the main drainage canal K1 to the right branch of the main irrigation canal C2. The eastern boundary of the model followed the main irrigation canal C2 (right branch), and the northern boundary was assigned along the northern main drainage canal K4. The bottom boundary of the model was the low Quaternary–Neogene dense clay of low permeability. The mean depth of the bottom boundary of the model was 51 m. The east–west cross section of the model is presented in Figure 3.

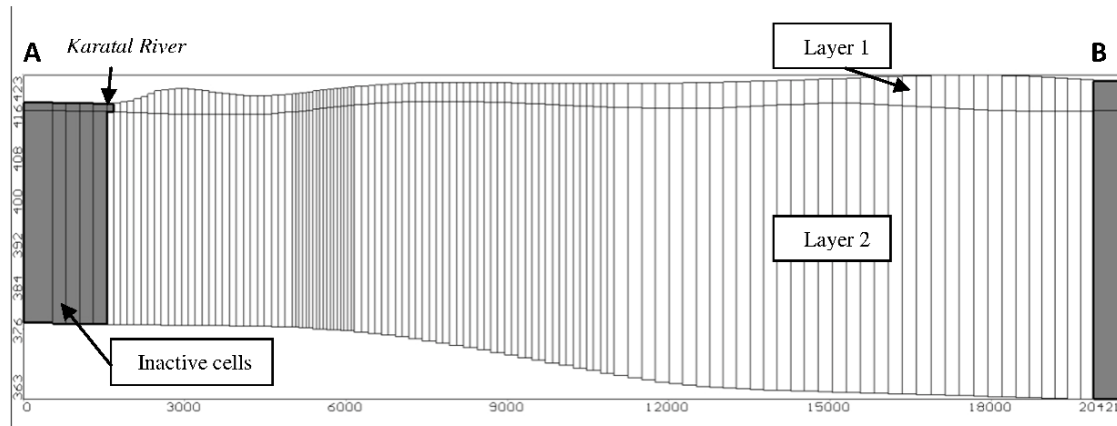


Figure 3. Geological cross-section of Karatal irrigated fields (cross-section line shown in Figure 2) with schematic demonstration of lithological layers

Storativity values for each layer were based on field and laboratory tests and were well aligned with typical values given in the Enviro-Base of Visual MODFLOW, according to the layer's lithology. Final storativity values were determined during the model calibration. To simulate the groundwater recharge due to rainfall and irrigation water, the Recharge Package of Visual MODFLOW (WHI, 2005) was used. The initial input values of groundwater recharge were based on the amount of irrigation and rainfall water and assigned as 10% of their amount. The actual recharge was estimated during the model calibration. To simulate recharge from the rice checks, the HGB Boundary Package module, supported by Visual MODFLOW, was used. The rate of water infiltration from the rice checks to the upper aquifer was assumed to be proportional to the difference in water head of the filled rice check and the elevation of the check bottom. The conductance value of the check bottom depends on the hydraulic conductivity, the area of the check and thickness of the bottom layer. However, this specific formulation requires detailed information which was not available. The initial input values of the hydraulic conductivity were based on experimental data of water loss from rice checks in the irrigated area and defined as  $0.01 \text{ m day}^{-1}$ . To account for the end of water infiltration after drying of the rice checks, the hydraulic conductivity values were significantly decreased to  $1 \times 10^{-7} \text{ m day}^{-1}$ .

To simulate evaporative losses from a shallow groundwater table, the Evaporation Package of Visual MODFLOW was used. The initial input values were based on actual local meteorological evaporation data and applied uniformly over the model with an extinction depth of 1.5 m.

The Karatal River and main drainage canals K1 and K4 were simulated using the River Boundary Package (RBP) module supported by Visual MODFLOW. The RBP simulates the water exchange between surface water in the river and groundwater in the aquifer. If the water level in the river is above the groundwater table in the coastal zone, the river recharges the groundwater; otherwise, it drains the groundwater. In accordance with the hydrograph and bottom profile of the Karatal River and main canals, their length was divided into several bank sites; a linearly varying level of surface water was prescribed for each of them.

We calibrated the model for the period January 2011 to January 2013, when the observations were carried out. During calibration, the model parameters were adjusted until good agreement was achieved between the simulated and measured head values. Wherever simulated hydraulic heads did not match the observed values, careful adjustments were progressively made of the hydraulic conductivity and water-budget values in the model layers and the relevant grid cells. Model calibration was continued until an acceptably significant match between simulated and observed behaviors was achieved. The accepted accuracy of the model calibration in terms of water levels was defined as 0.5 m, whereas in terms of groundwater budget components it was 10%. To understand which parameters are most and least likely to affect the model results, a sensitivity analysis was performed as part of the calibration procedure.

### 2.2.5 Simulation Scenarios

The model was applied to simulate the design of a planned infiltration pool for artificial groundwater recharge to solve water-supply problems for the Kishi-Tobe agricultural settlement. Using this model, the following forecast

scenarios were solved.

The first scenario aimed to assess the changes in the groundwater regime while specifying infiltration pool size, location, and mode of infiltration during the 10-year forecast period. One infiltration pool with a bottom size of 100 x 100 m and 1.0 m depth was set at the upper layer of model. The hydraulic conductivity value of the infiltration-pool bottom was set at  $2.2 \text{ m day}^{-1}$ . The initial value of the infiltration rate based on preliminary estimates was set to equal  $0.5 \text{ m day}^{-1}$  or  $5000 \text{ m}^3 \text{ day}^{-1}$ . Thus, the additional groundwater recharge at the model cells under the pool was set to the rate of  $30\ 500 \text{ mm year}^{-1}$  in each of the six model cells of the pool bottom. The recharge was set for 6 months per year during the following periods: March–April; June–July; October–November. Thus, the prescribed total volume of additional groundwater recharge from the infiltration pool was  $900\ 000 \text{ m}^3$  or 2.5% of the total water supply for irrigation. The minimum technically feasible distance of the pool from the Kishi-Tobe settlement was taken into account following the general plan of its development up until 2030. The minimal thickness of the soil cover deposits with low permeability also accounted for the infiltration pool location. If simulated groundwater levels reached the ground surface near the infiltration pool, then the value of the recharge was overestimated and had to be decreased to decrease groundwater level.

The second scenario aimed to evaluate the capacity of groundwater resources for supplying the water required by the Kishi-Tobe settlement under conditions of artificial recharge from the pool. The problem was reduced to a calculation of groundwater drawdown in the pumping-well locations at the end of the 10-year forecast period. Pumping was simulated from two pumping wells, with the same pumping rate set for both wells. It was gradually increased from  $216 \text{ m}^3 \text{ day}^{-1}$  to  $432 \text{ m}^3 \text{ day}^{-1}$  at the beginning and end of the forecast period, respectively, reflecting the planned increase in water consumption. Continuous and simultaneous pumping from both wells was planned continuously and simultaneously for all 10 years of the forecast period. Well depth was 48 m; well screens were set in the second layer of the model at depth intervals of 30–35 m and 38–42 m, while total pumping rate was divided equally for each interval. The distance between the wells was 40 m. The wells were located at a distance of 350 m from the pool in the northwest direction downstream of the groundwater flow. Positions of the pumping wells were assigned in accordance with the existing development plan.

The third scenario aimed to estimate the potential rates of groundwater pumping under the maximum allowable groundwater drawdown at the pumping-well locations at the end of the 10-year forecast period for the conditions of artificial recharge from the pool. The maximum allowable groundwater drawdown in the water-pumping wells to the end of the 10-year forecast period was 24 m, which is 50% of the average thickness of the lower aquifer. Two pumping wells (located as in the second scenario) were set in the model as "Constant Head" boundary conditions, with groundwater head elevation of 10 m depth from soil surface; adjustments were made by relating the model cell size to the real well diameter based on Theis's solution (Theis, 1935). The infiltration pool was set as in the first scenario. All other parameters of the model were the same as those obtained from the calibration process.

### 3. Results and Discussion

Results from the sensitivity analysis indicated that the model is relatively insensitive to changes in specific storage (initial values  $\pm 20\%$ ) and hydraulic conductivity values (initial values  $\pm 50\%$ ). At the same time, changes in groundwater-recharge values due to infiltration of the irrigation water produced a significant fit to the groundwater head contours. The results of the model calibration for January 2013 (730 days from the beginning of the model calibration) are shown in Figure 4.

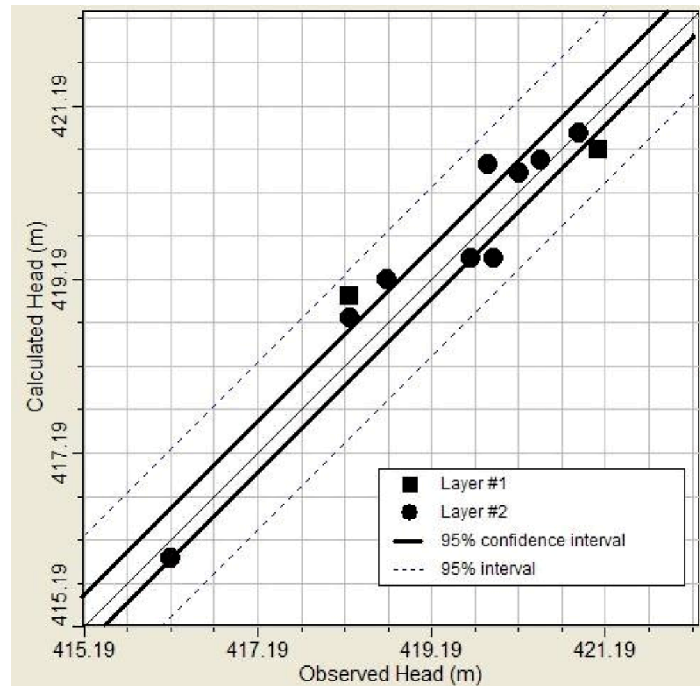


Figure 4. Model calibration: calculated vs. observed heads for January 2013

The standard error of the hydraulic head was 0.103 m and the normalized root mean square (RMS) was 8.99%. The hydraulic conductivity values of the model layers calculated during model calibration were compared with the initial values based on pumping in the observation wells and double-ring infiltrometer tests. For the bottom sediments of the Karatal River and the main drainage canals, the hydraulic conductivity was  $0.001 \text{ m day}^{-1}$ , with a bottom sediment thickness of 0.5 m. Figures 5 and 6 present a comparison between calculated and measured groundwater levels in observation wells 130 and 132, respectively.

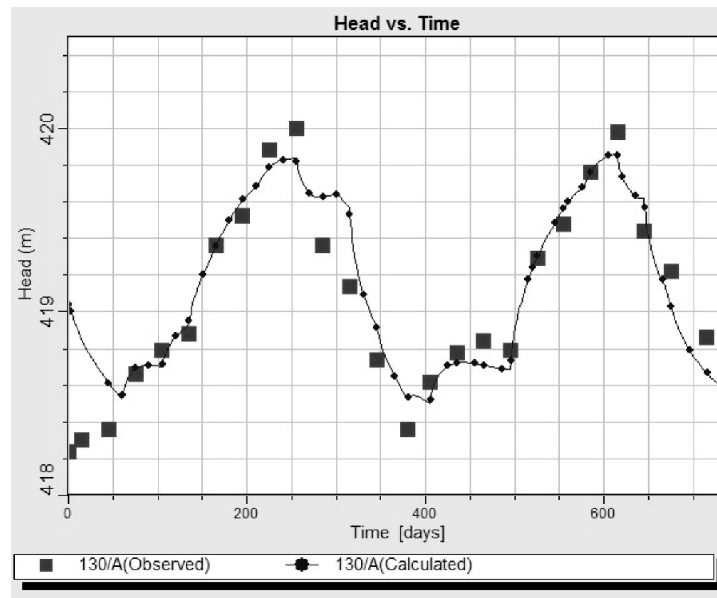


Figure 5. Model calibration: temporal changes in observed and simulated groundwater heads in observation well 130, January 2011–January 2013, located in the upper unconfined aquifer (Layer 1)

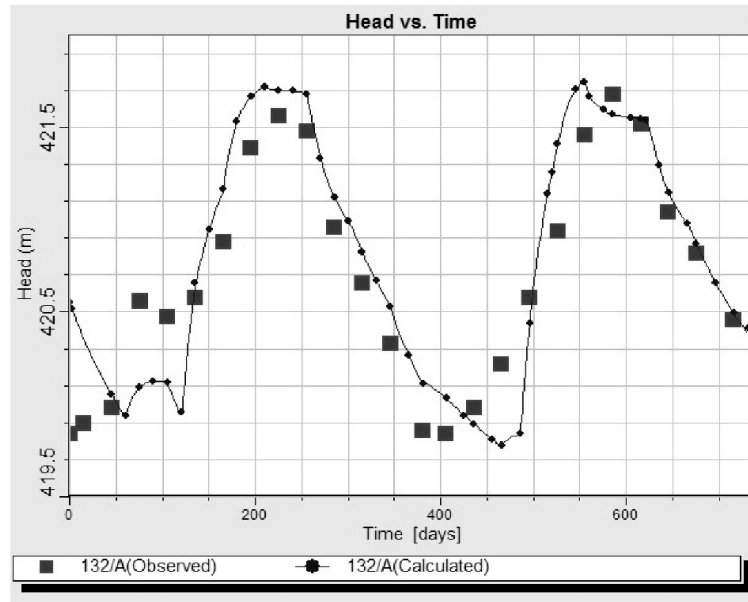


Figure 6. Model calibration: temporal changes in observed and simulated groundwater heads in observation well 132, January 2011–January 2013, located in the semi-confined aquifer (Layer 2)

Observation well 130 (6 m deep) characterized the groundwater heads in the upper unconfined aquifer (Layer 1); observation well 132 (10 m deep) characterized the groundwater heads in the semi-confined aquifer (Layer 2). Both observation wells were located within the irrigated field's area. There was good agreement between the observed and modeled head values.

Figure 7 shows simulated groundwater head equipotentials and groundwater velocity vectors for the unconfined aquifer (model Layer 1) in March 2012, before irrigation began.

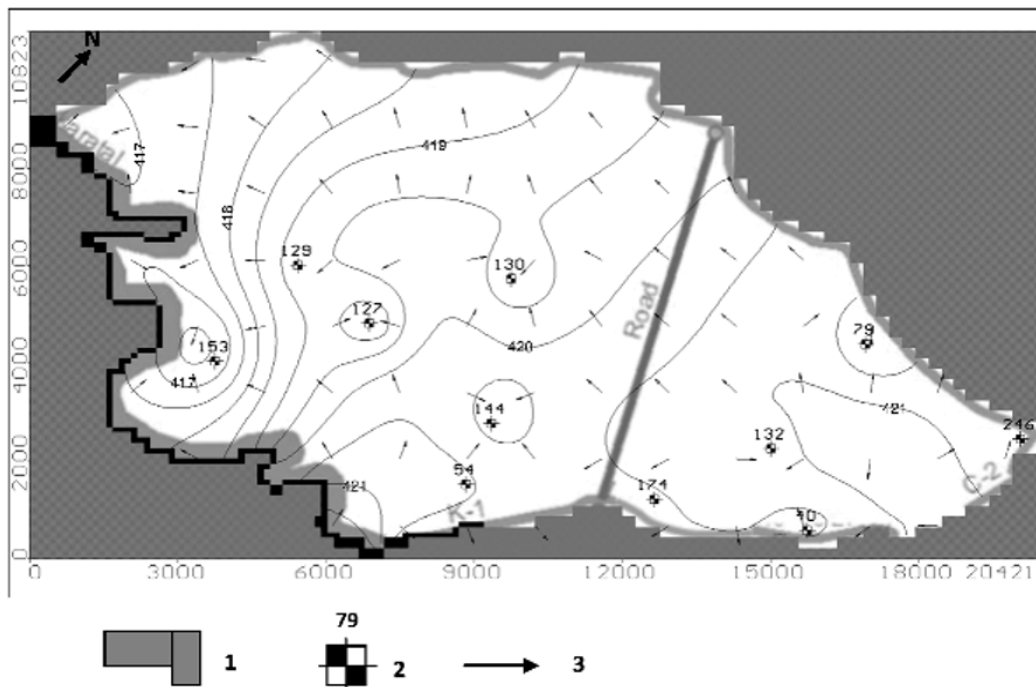


Figure 7. Groundwater head equipotentials and groundwater velocity vectors in Layer 1 in March 2012. Numbers in legend indicate the following locations on the map: 1 = inactive cells (no flow within model domain); 2 = observation well; 3 = velocity vector

The flow patterns were similar to the semi-confined aquifer (model Layer 2), with a general flow direction to the Karatal River (draining groundwater regionally). The hydraulic gradient was approximately  $2.5 \times 10^{-4}$  [m/m] in most of the area and gradually increased toward the river.

Draining impact of the main canals on the groundwater was only manifested at close vicinity. By mid-summer, intensive irrigation significantly changed the groundwater flow patterns (Figure 8).

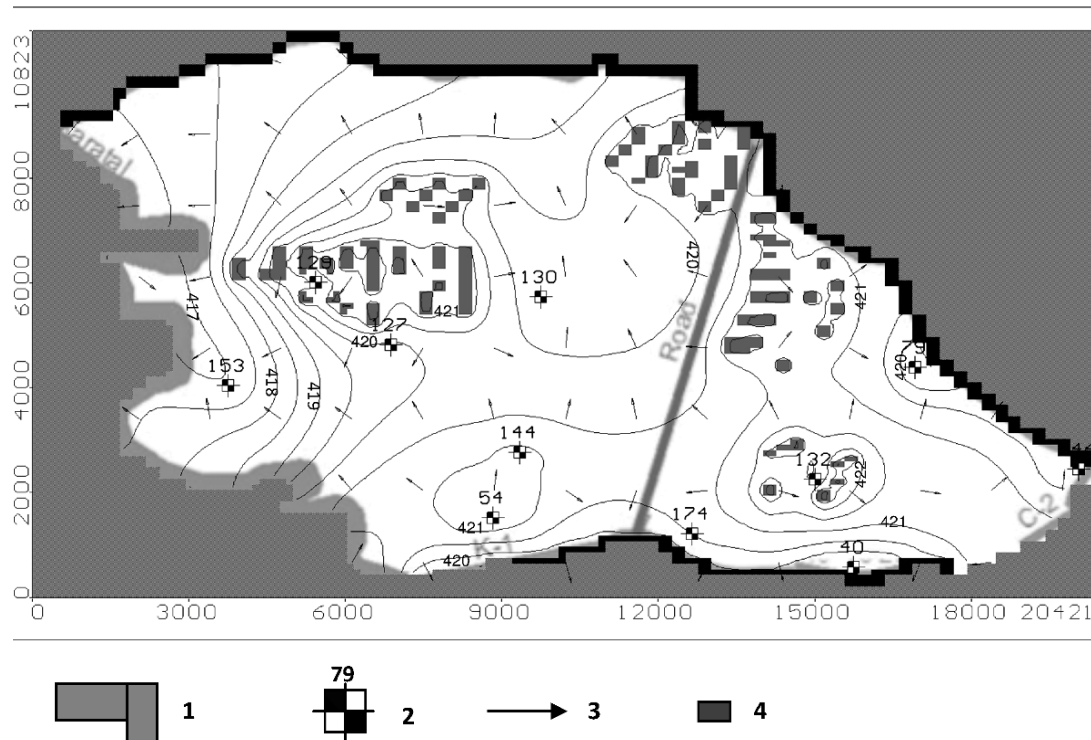


Figure 8. Groundwater head equipotentials and groundwater velocity vectors in Layer 2 in July 2012 (intensive irrigation). Numbers in legend indicate the following locations on the map: 1 = inactive cells (no flow within model domain); 2 = observation well; 3= velocity vector; 4 = rice checks

A groundwater mound developed under and around the flooded rice fields. The hydraulic gradient near the rice checks increased and the groundwater flowed not only to the Karatal River, but also toward the main drainage canals.

The groundwater-flow balance for the Karatal-irrigated fields was calculated for three periods in 2012: March – before irrigation; July – under irrigation and rice-check filling, and October – after irrigation and rice-check drying (Table 1).

Table 1. Groundwater-flux balance in the Karatal agricultural area calculated for March, July and October 2012. Results of the model calibration

Components of the balance	Inflow ( $\text{m}^3 \text{ day}^{-1}$ )	Percent of total	Outflow ( $\text{m}^3 \text{ day}^{-1}$ )	Percent of total
March 2012 (425 days)				
Recharge (rainfall and irrigation)	2443	48.8	–	–
Infiltration from Karatal River and main irrigation canals	2485	49.7	–	–
Infiltration from rice checks	74	1.5	–	–
Evapotranspiration	–	–	6297	82

Discharge to Karatal River and drainage system	–	–	1381	18
Total	5002	100	7678	100
$\Delta$ (Inflow – Outflow)	-2676 (-53.4% from total inflow)			
July 2012 (545 days)				
Recharge (rainfall and irrigation)	45 006	42.1	–	–
Infiltration from Karatal River and main irrigation canals	828	0.8	–	–
Infiltration from rice checks	60 996	57.1	–	–
Evapotranspiration	–	–	90 015	94
Discharge to Karatal River and drainage system	–	–	5704	6
Total	106 830	100	95 719	100
$\Delta$ (Inflow – Outflow)	11 111 (10.4% from total inflow)			
October 2012 (635 days)				
Recharge (rainfall and irrigation)	28 859	88.4	–	–
Infiltration from Karatal River and main irrigation canals	3713	11.4	–	–
Infiltration from rice checks	52	0.2	–	–
Evapotranspiration	–	–	92 804	95.6
Discharge to Karatal River and drainage system	–	–	4288	4.4
Total	32 624	100	97 092	100
$\Delta$ (Inflow – Outflow)	-64 468 (-197.6% from total inflow)			

According to Table 1, the calculated groundwater-flow balance for March 2012 gave a total inflow rate of 5002  $\text{m}^3 \text{day}^{-1}$ ; 49.7% of this was received by infiltration of the surface water from the Karatal River and 82% of the outflow was due to evaporation in the areas with a shallow groundwater table. The negative difference between inflow and outflow in the groundwater-flow balance was compensated for by drainage of the upper aquifer under the irrigated fields. As a result, there was a decrease in the groundwater level in the area. During irrigation and rice-check filling (Table 1, July), the total inflow rate of the groundwater flux increased dramatically. The main sources of the inflow were irrigation of associated crops and water infiltration from rice checks. The main part of the outflow rate of the groundwater flux was due to evaporation, and 6% was drained by the drainage system and Karatal River. A positive difference between inflow and outflow in the groundwater-flux balance was compensated for by filling of the upper aquifer under the irrigated fields. As a result, groundwater levels rose in the area. In October, after the irrigation period and rice-check drying, the total inflow rate of the groundwater flux decreased. At the same time, evaporation in areas with shallow groundwater remained very intensive. Again, the negative difference between inflow and outflow in the groundwater-flow balance was compensated for by draining of the upper aquifer under irrigated fields and rice checks. The performance of the groundwater-flux balance was typical for areas with rice-check irrigation (Veselov, Begaliev, & Samoukova, 1996).

The maximum allowable value of additional artificial groundwater recharge from the infiltration pool estimated in the first scenario was 1000  $\text{m}^3 \text{day}^{-1}$ . For the initially prescribed infiltration-rate value (5000  $\text{m}^3 \text{day}^{-1}$ ), groundwater levels rose up to soil surface shortly after the start of the first infiltration cycle in an area with a radius of 500 m from the center of the infiltration pool. Figure 9 shows the relationship between groundwater levels and distance from the center of the infiltration pool for the prescribed infiltration rate of 1000  $\text{m}^3 \text{day}^{-1}$ .

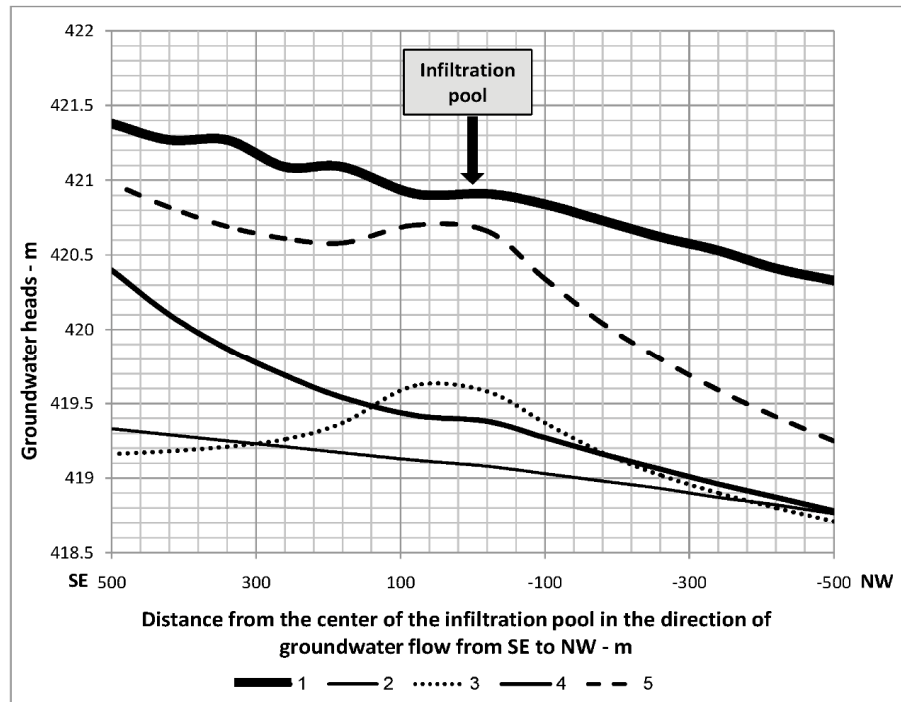


Figure 9. Groundwater heads at different distances from the center of the infiltration pool before and after 1st and 2nd infiltration cycles for an infiltration rate of  $1000 \text{ m}^3 \text{ day}^{-1}$ . 1 = Soil surface; 2 = groundwater heads before 1st infiltration cycle; 3 = groundwater heads upon completion of 1st infiltration cycle; 4 = groundwater heads before 2nd infiltration cycle; 5 = groundwater heads upon completion of 2nd infiltration cycle

Simulation results indicated that the radius of the groundwater mound does not exceed 500 m from the center of the infiltration pool (Figure 10).

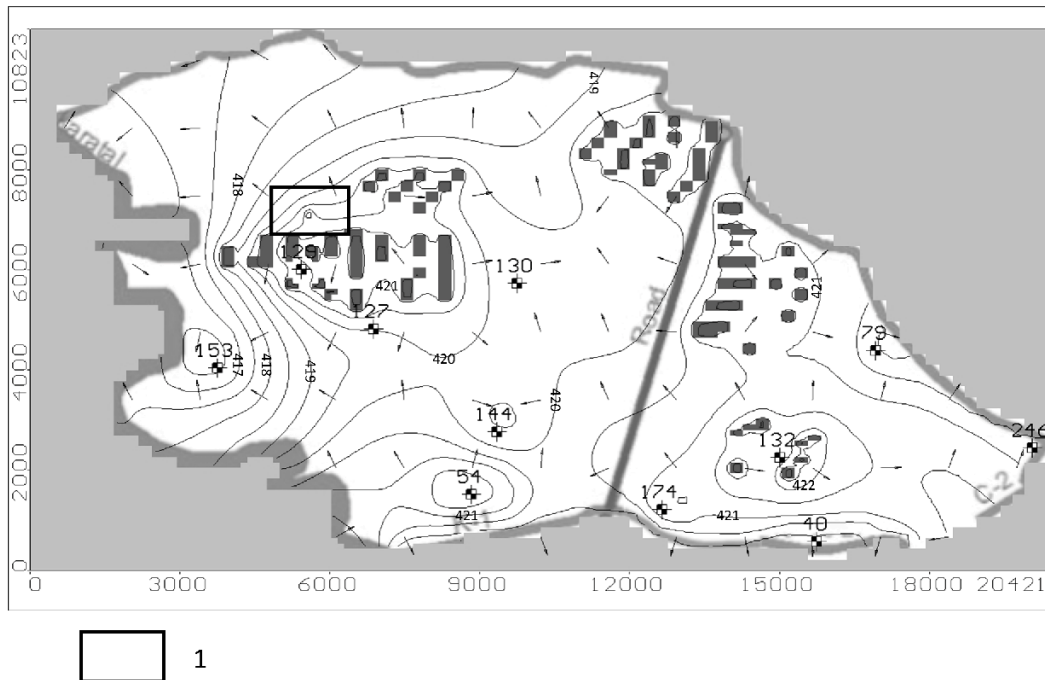


Figure 10. Predicted groundwater head equipotentials and flow velocity vectors in Layer 1 in July (intensive irrigation) under artificial groundwater recharge from infiltration pool. 1 = Contour of zoomed area of infiltration pool site (see Figure 11). The remaining symbols are as in Figure 8

The groundwater heads in the upper aquifer under the infiltration pool reached a maximum after the second cycle of infiltration (June–July), together with an overall rise in groundwater level in the middle of the irrigation period. Figure 11 clearly demonstrates that development of a groundwater mound impedes the motion of the regional groundwater flow from rice checks to the northwest.

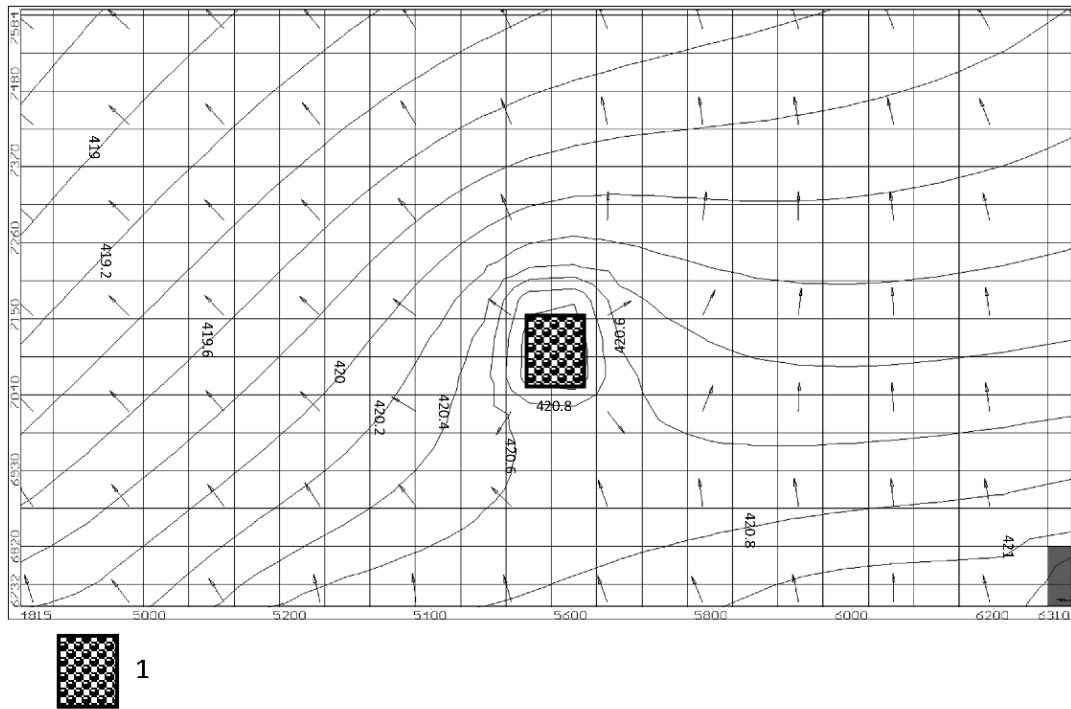


Figure 11. Zooming in (from Figure 10) on groundwater head equipotentials and flow velocity vectors in Layer 1 in July (intensive irrigation) under artificial groundwater recharge from infiltration pool. 1 = Infiltration pool

The time lag in the groundwater-level rise from the start of the infiltration cycle depended on the depth of the groundwater level (unsaturated zone thickness) under the pool (Figure 12)

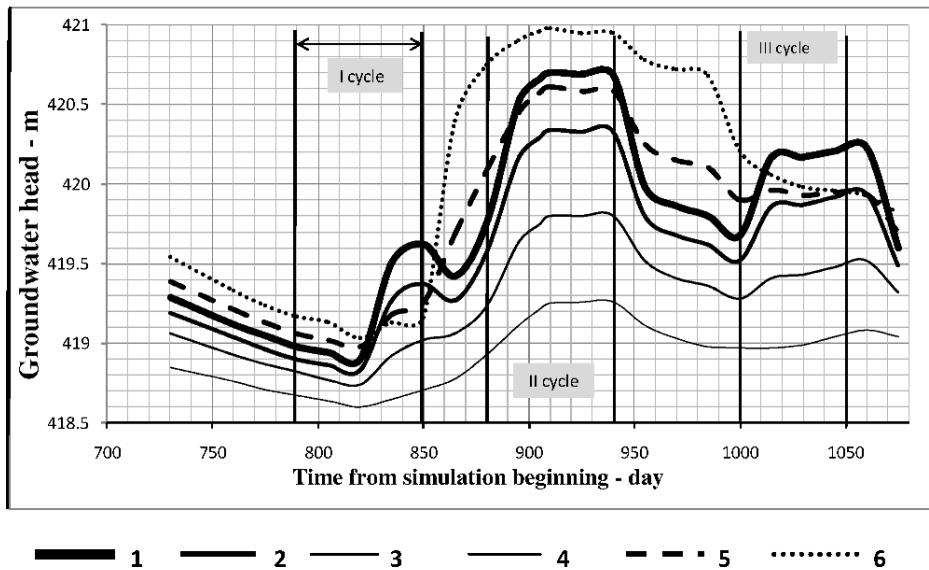


Figure 12. Predicted groundwater heads at different distances from infiltration pool during 1st year of infiltration cycles. 1 = Center of infiltration pool; 2, 3, 4 = 100 m, 260 m, 500 m, respectively, from infiltration pool downstream of groundwater flow; 5 and 6 = 260 m and 500 m from infiltration pool upstream of groundwater flow

Before the first (spring) infiltration cycle, when the depth of the groundwater table under the pool was around 2 m, the simulated time lag was 20–25 days. Before the second infiltration cycle, the groundwater table was at a depth of 1.1–1.2 m below the pool bottom, and a rise in groundwater level due to seepage from the pool took place almost immediately after infiltration started, causing an overall rise in groundwater level in the area under irrigation. Before the third (autumn) infiltration cycle, the high groundwater level persisted under the pool at a depth of 1.3 m. It was expected that groundwater levels would begin to rise soon after the start of infiltration, causing a gradual increase in water level at some distance around the pool.

The groundwater balance is expected to change significantly due to infiltration from the pool. Zooming in on the area of the infiltration pool location, Table 2 demonstrates groundwater balances calculated prior to the infiltration cycles and at the end of the infiltration cycles for the first year and 10th year of the prediction.

Table 2. Groundwater flux balance in the area of influence of the infiltration pool calculated prior to the start and at the end of infiltration cycles for 1st year and 10th year of prediction (numbers in parentheses). Results of model simulation according to first scenario

Components of the balance	In (m <sup>3</sup> day <sup>-1</sup> )	Percent of total	Out (m <sup>3</sup> day <sup>-1</sup> )	Percent of total
Prior to start of 1st infiltration cycle				
Recharge (rainfall and infiltration from the pool)	1.9 (0)	73 (0)	–	–
Flow across the outer boundary of the area	0.7 (0.6)	27 (100)	301.1 (185.6)	100 (100)
Evapotranspiration				
Total	2.6 (0.6)	100 (100)	301.1 (185.6)	100 (100)
Δ (Inflow – Outflow)				-298.5 (-185)
End of 1st infiltration cycle				
Recharge (rainfall and infiltration from the pool)	1125 (1125)	93 (94.6)	–	–
Flow across the outer boundary of the area	85.2 (64.3)	7 (5.4)	989.2 (992.8)	99.7 (99.3)
Evapotranspiration			2.75 (6.4)	0.3 (0.7)
Total	1210.2 (1189.3)	100 (100)	991.95 (999.2)	100 (100)
Δ (Inflow – Outflow)				218.25 (190.1)
Prior to start of 2nd infiltration cycle				
Recharge (rainfall and infiltration from the pool)	123.9 (123.9)	10.7 (11.6)	–	–
Flow across the outer boundary of the area	1034.8 (944.7)	89.3 (88.4)	4 (4.3)	3 (2.5)
Evapotranspiration			130.2 (159.8)	97 (97.3)
Total	1158.7 (1068.6)	100 (100)	134.2 (164.1)	100 (100)
Δ (Inflow – Outflow)				1024.5 (904.5)
End of 2nd infiltration cycle				
Recharge (rainfall and infiltration from the pool)	1309.7 (1309.7)	54.6 (48.9)	–	–
Flow across the outer boundary of the area	1090.6 (1370.3)	45.4 (51.1)	940.7 (922.3)	48.5 (54.5)
Evapotranspiration			997.3 (769.4)	51.5 (45.5)
Total	2400.3 (2680)	100 (100)	1938 (1691.7)	100 (100)
Δ (Inflow – Outflow)				462.3 (988.3)
Prior to start of 3rd infiltration cycle				
Recharge (rainfall and infiltration from the pool)	2.5 (2.5)	0.7 (0.6)	–	–
Flow across the outer boundary of the area	141.8 (150.2)	98.3 (98.4)	84 (68.5)	10.2 (8.4)
Evapotranspiration			735.5 (744.9)	89.8 (91.6)
Total	144.3 (152.7)	100 (100)	819.5 (813.4)	100 (100)
Δ (Inflow – Outflow)				-675.2 (-660.7)
End of 3rd infiltration cycle				
Recharge (rainfall and infiltration from the pool)	1325.1 (1325)	98.2 (99.8)	–	–
Flow across the outer boundary of the area	23.6 (3)	1.8 (0.2)	1071 (1148)	86.1 (86.5)

Evapotranspiration			172.5 (178.8)	13.9 (13.5)
Total	1358.2 (1370.7)	100 (100)	1357.3 (1370.9)	100 (100)
$\Delta$ (Inflow – Outflow)			105.2 (1.2)	
At the end of the year (December)				
Recharge (rainfall and infiltration from the pool)	92.1 (92.1)	99.2 (99.2)	–	–
Flow across the outer boundary of the area	0.7 (0.7)	0.8 (0.8)	426.5 (467.9)	97.6 (98.1)
Evapotranspiration			10.5 (9)	2.4 (1.9)
Total	92.8 (92.8)	100 (100)	437 (476.9)	100 (100)
$\Delta$ (Inflow – Outflow)			-344.2 (-384.1)	

We note that the values of the balance components within the forecast period (10 years) do not change substantially. The total groundwater flux in the area of the infiltration pool (Out) increased from 300 m<sup>3</sup> day<sup>-1</sup> prior to the first infiltration cycle to 1938 m<sup>3</sup> day<sup>-1</sup> at the end of the second infiltration cycle, and then decreased again to 437 m<sup>3</sup> day<sup>-1</sup> at the end of the year (December). During the infiltration cycles, a positive difference between inflow and outflow in the groundwater-flux balance was compensated for by filling of the upper aquifer. As a result, groundwater levels rose in the area and a groundwater mound formed under the infiltration pool.

Simulations of groundwater pumping during the 10-year forecast period for the second scenario showed that the radius of influence of the pumping well over 10 years would not exceed 300 m. This makes it possible to install two pumping wells at a distance of 40–50 m from each other with a small sanitary protection zone. Figure 13 demonstrates the relationship between groundwater pumping rate and drawdown.

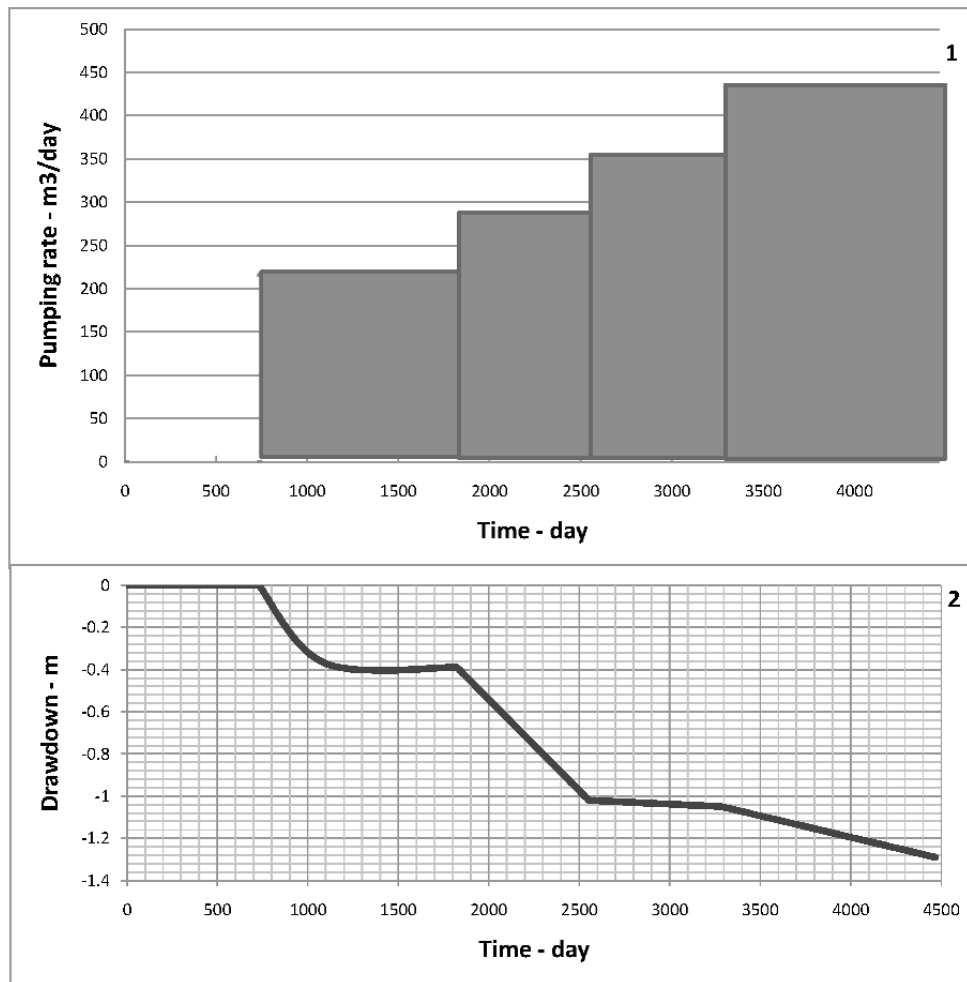


Figure 13. Pumping rate (1) and simulated groundwater drawdown (2) at pumping well for the 10-year forecast period (2nd task)

The simulated drawdown in the pumping wells was around 1.3–1.4 m; adjusting this value by relating the model cell size to the real well diameter gave an expected drawdown of 15–16 m. The total volume of the pumped water ( $3.6 \times 10^6 \text{ m}^3$  over 10 years) is 1% of the total volume of the groundwater balance.

According to the simulation results for the third scenario, the potential rates of groundwater pumping from two wells can reach  $7350 \text{ m}^3 \text{ day}^{-1}$ . The cone of depression in the groundwater table will expand in the northwest direction. The radius of the depression cone will reach 2.4 km after 10 years of pumping. The groundwater mound under the irrigated fields and rice checks will be superimposed on the depression cone. As a result, the cone of the groundwater depression will be asymmetric (Figure 14).

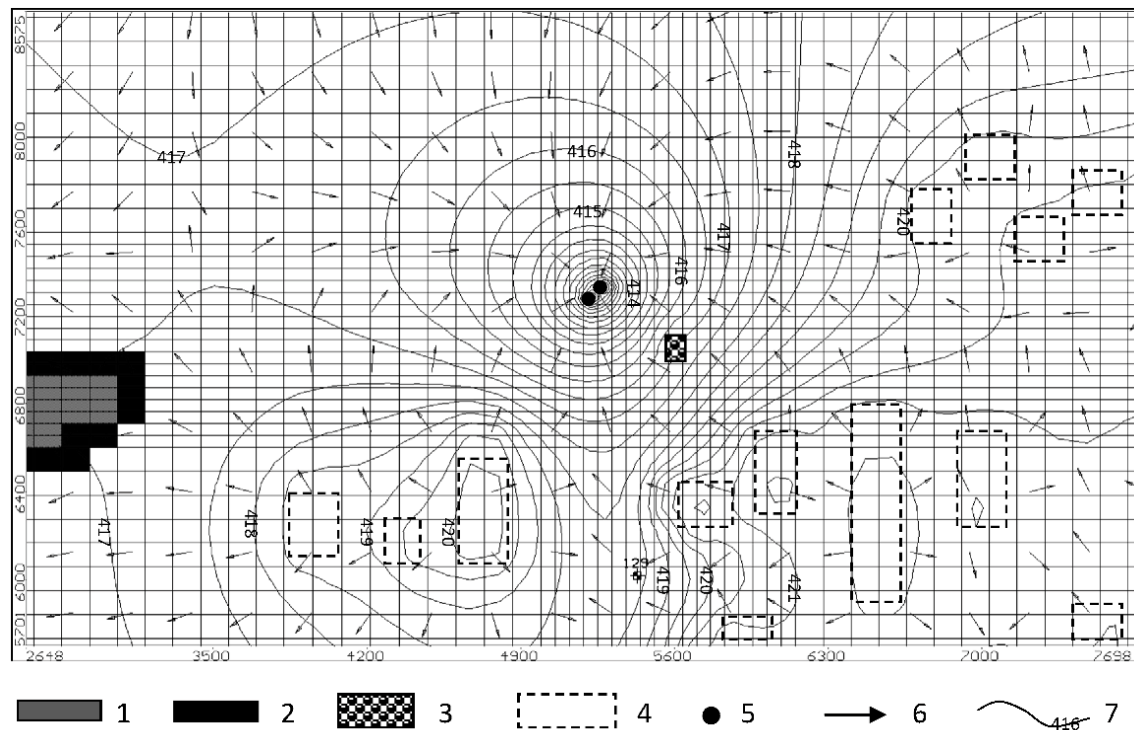


Figure 14. Predicted groundwater head equipotentials and flow velocity vectors in Layer 2 for 10-year forecast period in July (intensive irrigation) under artificial groundwater recharge from infiltration pool and groundwater pumping to fulfill maximum allowable groundwater drawdown at water pumping wells within the zoom contour.

1 = Inactive cells (no flow within model domain); 2 = Karatal River; 3 = infiltration pool; 4 = rice checks; 5 = pumping wells; 6 = flow-path direction; 7 = groundwater head equipotential

In this case, the total volume of supply-water pumped over 10 years will be  $26 \times 10^6 \text{ m}^3$ , which is 7.5% of the total volume of the groundwater-resource balance.

#### 4. Conclusions

1) A spatial-distribution groundwater-flow model such as MODFLOW can provide reliable information for the planning of artificial groundwater recharge from infiltration pools under complex hydrogeological and intensive farming conditions; in the future, such information might solve the water-supply problems of the local rural communities in the Karatal agricultural area in Kazakhstan.

2) The initial conceptualization of the hydrogeological system of the Karatal agricultural area—an unconfined–semi-confined two-layered aquifer sequence with different hydraulic characteristics—was confirmed by a reasonable match between the model and observed time-series water-level data.

3) Using a calibrated geofiltration model, the formation of a groundwater mound due to artificial groundwater recharge from an infiltration pool was studied. The maximum potential value of artificial groundwater recharge from the pool was determined to be  $1000 \text{ m}^3 \text{ day}^{-1}$ , with an infiltration layer of  $0.2 \text{ m day}^{-1}$ . The radius of the groundwater mound would not exceed 500 m from the center of the pool. In addition to its main function, the infiltration pool would prevent the inflow of contaminated groundwater from irrigated fields and rice checks to the pumping wells by developing a groundwater mound that acts as a hydrodynamic barrier to its movement.

- 4) The groundwater heads in the upper aquifer under the infiltration pool reached a maximum after the second cycle of infiltration (June–July). Development of a groundwater mound impedes the motion of the regional groundwater flow from rice checks to the northwest. The time lag in the groundwater-level rise from the start of the infiltration cycle depended on the depth of the groundwater level (unsaturated-zone thickness) under the pool. When the depth of the groundwater table under the pool was around 2 m, the simulated time lag was 20–25 days. At a groundwater table depth of 1.1–1.2 m below the pool bottom, a rise in groundwater level due to seepage from the pool occurred almost immediately after infiltration started, causing an overall rise in groundwater level in the area under irrigation.
- 5) The optimal location of pumping wells to supply drinking water to the Kishi-Tobe settlement under artificial recharge was confirmed.
- 6) The potential rates of groundwater pumping by two wells for the water supply can be up to  $7350 \text{ m}^3 \text{ day}^{-1}$  over a 10-year period. Maximum drawdown in wells in this case will be about 24 m. The required groundwater resource to supply water to the Kishi-Tobe settlement in the amount of  $864 \text{ m}^3 \text{ day}^{-1}$  is provided, in terms of both drawdown by the end of the forecast period, and balanced provision of the groundwater resource.

### Acknowledgements

This research was financed by the Ministry of Education and Science of the Kazakhstan Republic under research grant #38.61.05. We thank Ergan E. Kuldeev, pro-rector of Kazakhstan National Technical University in the name of K.I. Satpayev, for providing support throughout the duration of this study. We also thank Prof. Alexander Yakirevich for help in preparing this manuscript.

### References

- Al-Turbak, A. S. (1991). Effectiveness of recharge from a surface reservoir to an underlying unconfined aquifer. In EDITOR, *Hydrology of natural and manmade lakes: Proceedings of the 1991 IAHS Symposium* (Publ. no. 206). Vienna, Austria: IAHS.
- Bloyd, R. M. (1971). Underground storage of imported water in the San Gorgonio Pass area, southern California. USGS Water Supply Paper 1999-D. USGS.
- Bouwer, H. (2002). Artificial recharge of groundwater: Hydrogeology and engineering. *Hydrogeology Journal* 10, 121–142. <http://dx.doi.org/10.1007/s10040-001-0182-4>
- Evans, D. D., Young, D. W., & Onyskow, L. P. (1983). Hydrologic evaluations of small impoundments in arid and semiarid regions. Technical report for 1 Oct 1977–30 Sep 1979. National Technical Information Service (NTIS), No 8324, Springfield, VA.
- Fred, H. Jr. (2006). Artificial recharge of aquifers. Retrieved from [onlinelibrary.wiley.com/doi/10.1111/gwat.1963.1.issue-1/issuetoc2-8-2010](http://onlinelibrary.wiley.com/doi/10.1111/gwat.1963.1.issue-1/issuetoc2-8-2010)
- Gandy, C. J., Clarke, L., & Banks, D. (2010). Predictive modelling of groundwater abstraction and artificial recharge of cooling water. *Quarterly Journal of Engineering Geology and Hydrogeology* 43(3), 279–288. <http://dx.doi.org/10.1144/1470-9236/08-093>
- Gropius, M. (2010). Numerical groundwater flow and heat transport modelling of open-loop ground source heat systems in the London. *Quarterly Journal of Engineering Geology and Hydrogeology* 43(3), 23–32. <http://dx.doi.org/10.1144/1470-9236/08-105>
- Hashemi, H., Berndtsson, R., & Persson, M. (2014). Artificial recharge by floodwater spreading estimated by water balances and groundwater modeling. *Hydrological Sciences Journal*. <http://dx.doi.org/10.1080/02626667.2014.881485>
- Kavuri, M., Boddu, M., & Annamdas, V. G. M. (2011). *New methods of artificial recharge of aquifers: A review*. Poster presented at the 4th International Perspective on Water Resources & the Environment (IPWE), National University of Singapore (NUS), Singapore, 4–6 Jan 2011. Poster on Artificial Recharge of Aquifer, No. 1j.
- Khan, L., & Mawdsley, J. A. (1984). Method of predicting natural recharge of a groundwater basin. In *Fourth Congress – Asian and Pacific Division, IAHR* (pp. 1537–1552). Chiang Mai, Thailand.
- Koch, N. C. (1984). Simulated artificial recharge in the Big Sioux Aquifer in Minnehaha County, South Dakota. USGS Water-Resources Investigations Report 84-4312, p. 8.
- Kruseman, G. P., & De Ridder, N. A. (1976). *Analysis and evaluation of pumping test data* (p. 11). Wageningen, The Netherlands: International Institute for Land Reclamation and Improvement (ILRI).

- Mirlas, V. (2009). Applying MODFLOW model for drainage problem solution: A case study from Jahir irrigated fields, Israel. *Journal of Irrigation and Drainage Engineering* 135(3), 269–278. [http://dx.doi.org/10.1061/\(ASCE\)IR.1943-4774.0000003](http://dx.doi.org/10.1061/(ASCE)IR.1943-4774.0000003)
- Mirlas, V. (2012). Assessing soil salinity hazard in cultivated areas using MODFLOW model and GIS tools: A case study from the Jezre'el Valley, Israel. *Agricultural Water Management* 109, 144–154. <http://dx.doi.org/10.1016/j.agwat.2012.03.003>
- Mirlas, V. (2013). MODFLOW modeling to solve drainage problems in the Argaman date palm orchard, Jordan Valley, Israel. *Journal of Irrigation and Drainage Engineering* 139, 612–624. [http://dx.doi.org/10.1061/\(ASCE\)IR.1943-4774.0000593](http://dx.doi.org/10.1061/(ASCE)IR.1943-4774.0000593)
- Sanford, W. (2002). Recharge and groundwater models: An overview. *Hydrogeology Journal* 10, 110–120. <http://dx.doi.org/10.1007/s10040-001-0173-5>
- Shakibaev, I., Li, A., Kulagin, V., & Zaharova, N. (2013). Ameliorative condition of the irrigated fields in the Karatal irrigated area of Almaty region in 2011–2012. Technical report of the Zonal Hydrogeological-Ameliorative Center of Kazakhstan Republic, No. 24-35/4-191-5, Almaty, Kazahstan, p. 52 (in Russian).
- Theis, C. V. (1935). The relation between the lowering of the piezometric surface. *Transactions, American Geophysical Union* 16(2), 519–524.
- Valipour, M. (2012a). A comparison between horizontal and vertical drainage systems (include pipe drainage, open ditch drainage, and pumped wells) in anisotropic soils. *IOSR Journal of Mechanical and Civil Engineering* 4(1), 7–12. <http://dx.doi.org/10.9790/1684-0410712>, 2012
- Valipour, M. (2012b). Effect of drainage parameters change on amount of drain discharge in subsurface drainage systems. *IOSR Journal of Agriculture and Veterinary Science* 1(4), 10–18. <http://dx.doi.org/10.9790/2380-0141018>
- Valipour, M. (2013). *Comparison of different drainage systems usable for solution of environmental crises in soil*. Paper presented at the 1st International Conference on Environmental Crises and its Solutions, Kish Island, Iran. Abstract retrieved from [http://www.civilica.com/EnPaper-ICECS01-ICECS01\\_047.html](http://www.civilica.com/EnPaper-ICECS01-ICECS01_047.html)
- Valipour, M. (2014). *Handbook of drainage engineering problems*. Foster City, CA: OMICS Group eBooks.
- Veselov, V. V., Begaliev, A. G., & Samoukova, G. M. (1996). Ecological and ameliorative problems in usage of water resources in the Balkhash Lakebasin, Almaty, Gylm. ISBN 5-628-01999-2 (in Russian with English appendix).
- WHI (Waterloo Hydrogeologic, Inc.). (2005). *Visual MODFLOW, user's manual*, Professional Edition. Waterloo, Canada: WHI.

### Copyrights

Copyright for this article is retained by the author(s), with first publication rights granted to the journal.

This is an open-access article distributed under the terms and conditions of the Creative Commons Attribution license (<http://creativecommons.org/licenses/by/3.0/>).